Binding-potential modeling of the structural instability in $PrAg_{1-x}Cu_x$

I. Abu-Aljarayesh and J. S. Kouvel
Department of Physics, University of Illinois at Chicago, Chicago, Illinois 60680

T. O. Brun
Materials Science and Technology Division, Argonne National Laboratory, Argonne, Illinois 60439
(Received 19 February 1986)

The strong negative quadrupolar coupling in the isoelectronic pseudobinary $PrAg_{1-x}Cu_x$ compounds has been ascribed to a lattice instability of the cubic (CsCl) phase, which grows with increasing x and culminates in a transformation to an orthorhombic (FeB) phase at $x=0.5$. To probe the basis of this instability, the chemical binding of these compounds is modeled with Lennard-Jones–like potentials for the A-B, A-A, and B-B pair interactions (A = Pr, B = Ag or Cu). The numerical coefficients of the potentials are determined by minimizing the total binding energy with respect to the seven structural parameters of the orthorhombic phase. The BB potential is found to be negligibly weak, and the calculated AB and AA potentials, when applied to the cubic phase, reveal that the strong short-range A—B and A—A bonds are stretched and compressed, respectively. This structural frustration grows as x exceeds 0.5 and the cubic lattice parameter is allowed to decrease as Ag is further replaced by smaller Cu atoms. The pair-binding potentials are then used in determining the dynamical matrix of the cubic phase. The calculated phonon dispersion curves show that as x exceeds 0.5 there is a rapid softening of the TA_1 (C_{44}) mode, especially at the M ($\frac{1}{2}\frac{1}{2}0$) point. This zone-boundary phonon softening is shown to derive directly from the structural frustration and is consistent with the dominant internal static distortions involved in the cubic-to-orthorhombic transformation. It also supports the lattice-instability rationale for the strong antiferroquadrupolar coupling. However, it contrasts with the M-point softening of the TA_2 (C') mode previously observed in the isomorphic (but not isoelectronic) $LaAg_{1-x}In_x$ system, where the underlying mechanism is probably quite different.

I. INTRODUCTION

The CsCl-structured intermetallic compounds RAg, where R is a light rare-earth metal (La, Ce, or Pr), are known to have an appreciable lattice instability. In LaAg, inelastic neutron scattering experiments have revealed a partial softening of zone-boundary phonons,[1,2] while in CeAg and PrAg, ultrasonic velocity measurements indicate some softening of the same $TA_2(\zeta\zeta 0)$ mode.[3,4] Moreover, as the Ag in LaAg is progressively replaced by In, it was observed that the phonon softening increases, culminating (when the replacement reaches 0.1) in a cubic-to-tetragonal lattice transformation.[2,5] A similar transformation has been seen in $CeAg_{1-x}In_x$ and $PrAg_{1-x}In_x$ at low values of x.[6,7] However, the In substitution for Ag is not isoelectronic and thus may produce significant changes in the binding-electron density of states, which could well enhance the structural instability.[2,6,7]

In the case of PrAg, high-field magnetization measurements above the antiferromagnetic Néel temperature have disclosed the existence of a large negative (antiferro) quadrupolar coupling.[8,9] It was also found[8] that the strength of this coupling is essentially unchanged when the Pr in PrAg is partially replaced by nonmagnetic La and the bilinear exchange interactions are thereby reduced. Hence, it was concluded[8] that the quadrupolar coupling does not derive from higher-order exchange and that a probable alternative mechanism is a virtual phonon exchange process[10] driven by a lattice instability. This reasoning was later extended to the isoelectronic compounds $PrAg_{1-x}Cu_x$, for which similar magnetic measurements showed that as x is raised the negative quadrupolar coupling increases rapidly in strength while the bilinear exchange slowly diminishes.[11,12] Consistent with the possibility of a growing lattice instability, these changes were seen to continue until, at $x=0.5$, a transformation takes place upon cooling from the cubic CsCl-type structure to an orthorhombic FeB-type structure, as determined by neutron diffraction.[11]

A detailed comparison of the two crystal structures of $PrAg_{0.5}Cu_{0.5}$ revealed that the cubic-to-orthorhombic transformation may be regarded in terms of certain sets of alternating static displacements of parallel atomic planes.[11] These atomic displacements, if considered as dynamic phenomena, would correspond to zone-boundary phonons of appropriate wave vector to produce, via virtual phonon exchange, the strong negative quadrupolar interactions found in cubic $PrAg_{1-x}Cu_x$ of lower x. Moreover, as we will describe later, the symmetry of these hypothetical phonons at $\frac{1}{2}\frac{1}{2}0$ is that of the TA_1 (C_{44}) mode rather than the TA_2 (C') mode which softens in $PrAg_{1-x}In_x$. Hence, the lattice instability in $PrAg_{1-x}Cu_x$ may be quite different, and this interesting possibility needs to be checked by inelastic neutron scattering experiments when single-crystal samples of sufficient size become available.

Pending such experiments, we considered the alternative strategy of fully exploiting all the available structural information on the orthorhombic and cubic phases of $PrAg_{0.5}Cu_{0.5}$ in order to determine theoretically approximate phonon dispersion curves for cubic $PrAg_{1-x}Cu_x$. As a first step in this determination, pair-binding potentials of simple assumed form can be deduced for the orthorhombic phase of $PrAg_{0.5}Cu_{0.5}$ by free-energy minimization with respect to each of its seven structural parameters, whose values are known experimentally.[11] Since the cubic-to-orthorhombic transformation of this compound involves essentially no change in volume and presumably only very small changes in the self-consistent muffin-tin potentials for the electronic band structure,[13] it can be assumed that the pair-binding potentials also are relatively unaffected by the transformation. Secondly, since the $PrAg_{1-x}Cu_x$ compounds of various x are isoelectronic, simple modifications of the binding potentials can be made for different compositions, taking into account only the variation of the cubic lattice parameter resulting from the different atomic sizes of Ag and Cu. The phonon dispersion can then be calculated from the binding potentials for the different compositions in order to reveal any significant trends towards a lattice instability in cubic $PrAg_{1-x}Cu_x$.

We have followed this procedure and, in Sec. II, our results are presented for the binding potentials determined for $PrAg_{1-x}Cu_x$, first for $x=0.5$ and later extended to other compositions. Within the virtual-crystal approximation (where the Ag and Cu atoms occupying the same type of lattice sites at random are treated collectively), it is found that the Ag(Cu)—Ag(Cu) bonds are negligibly weak and that, in the cubic CsCl-type structure, the Pr—Ag(Cu) and Pr—Pr bonds are stretched and compressed, respectively, constituting a "structural frustration" which grows with increasing x. In Sec. III we present our calculated phonon dispersion curves for cubic $PrAg_{1-x}Cu_x$, which reveal that as x increases beyond 0.5 there is a rapid softening of the $TA_1(\zeta\zeta 0)$ mode, especially at the M $(\frac{1}{2}\frac{1}{2}0)$ point. It is shown that this lattice instability derives from the structural frustration and that it is consistent with the internal atomic displacements that accompany the transformation to the orthorhombic FeB-type structure. Some concluding remarks are given in Sec. IV.

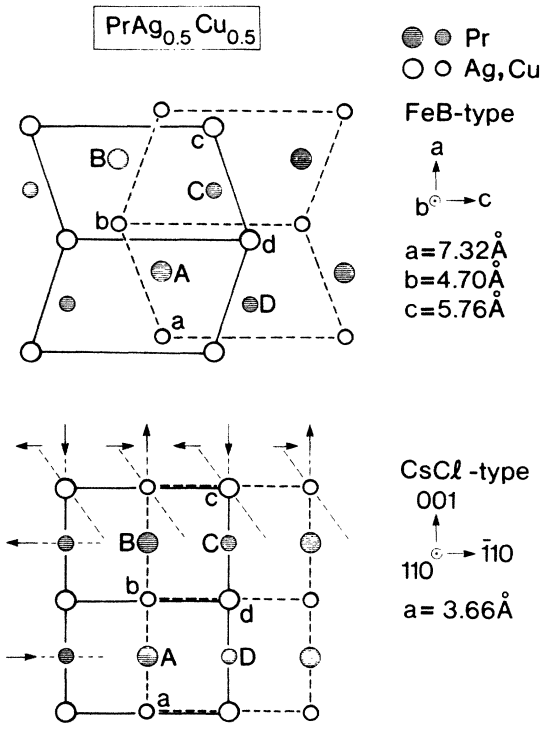

FIG. 1. Orthorhombic FeB-type and cubic CsCl-type structures of $PrAg_{0.5}Cu_{0.5}$, with lattice parameters as shown. The internal parameters of the FeB-type (*Pnma*), involving atomic degrees of freedom in the *ac* plane, are for Pr in 4*c* sites, $x_A=0.179$ and $z_A=0.136$, and for Ag or Cu atoms in 4*c* sites, $x_B=0.034$ and $z_B=0.641$. The y_A and y_B parameters are fixed at $\frac{1}{4}$ by symmetry. Other features are described in the text.

II. PAIR-BINDING POTENTIALS

In obtaining pair-binding potentials for $PrAg_{1-x}Cu_x$, we first consider the $x=0.5$ compound which undergoes a cubic-to-orthorhombic transformation upon cooling. The cubic CsCl-type and orthorhombic FeB-type structures of this compound, as determined by neutron diffraction,[11] are displayed in Fig. 1. They are drawn to scale for the lattice and internal parameters indicated and are projected on the (110) and *ac* planes, respectively. In these projections, all the atoms lie on alternating equally spaced levels of two kinds and are so designated by the large and small circles. In the orthorhombic unit cell, the four different sites occupied by Pr (shaded circles) are labeled A,B,C,D and the four different sites occupied randomly by Ag or Cu (open circles) are labeled a,b,c,d; this labeling is carried over to the corresponding sites in the cubic structure. In the latter, the arrows shown represent alternating displacements of three sets of parallel atomic planes normal to the (110) plane, whose sum (plus uniform distortions) succeeds in converting the CsCl-type structure to the FeB-type structure. As pointed out previously,[11,12] if any of these sets of static displacements are regarded as dynamic, they would represent zone-boundary phonons, whose softening may well describe the lattice instability of the CsCl-type structure. This observation will later be shown to be confirmed by our phonon-dispersion calculations.

Our interest at this stage, however, is in how the CsCl→FeB transformation of $PrAg_{0.5}Cu_{0.5}$ translates quantitatively into changes in the interatomic spacings. Using the experimental values for the lattice parameters (and the internal parameters of the FeB-type structure), as given in Fig. 1 and its caption, we have calculated the separation distances between a Pr or Ag (Cu) atom and its various neighboring atoms in both structures. The interatomic distances are displayed in Fig. 2, where those for the FeB structure are linked to those for the CsCl structure (out to third nearest neighbors), following the atomic correspondences indicated by the labeling in Fig. 1. These distances, to which all our calculations were subsequently restricted, are specified more exactly in Appendix A. Qualitatively, regarding the interatomic separations of

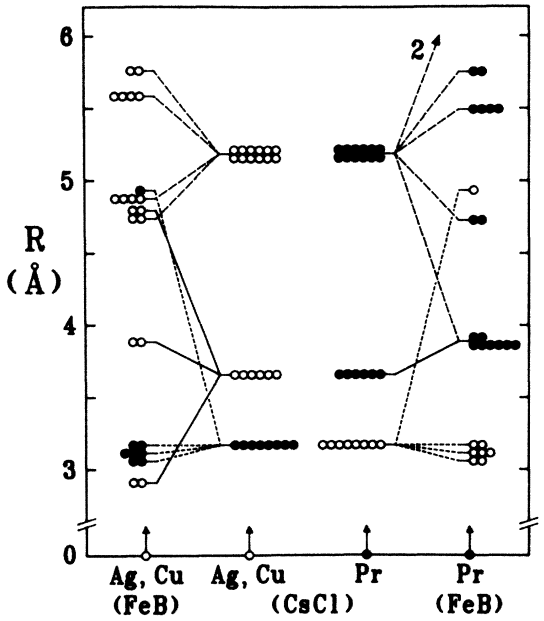

FIG. 2. Interatomic distances (in Å) in the FeB-type and CsCl-type structures of $PrAg_{0.5}Cu_{0.5}$. The number of neighbors at the same (or nearly the same) distance from a Pr or Ag or Cu atom is indicated.

short range, it is clear from Fig. 2 that the cubic-to-orthorhombic transition produces a reduction of the average Pr—Ag(Cu) distance (except for one greatly increased pair separation) and an enlargement of the average Pr-Pr distance, while the Ag(Cu)—Ag(Cu) distances show no predominant direction of change.

We will now assume that the *A-B*, *A-A*, and *B-B* pair interactions (where A = Pr, B = Ag or Cu) can be adequately represented by spherically symmetric potentials of a Lennard-Jones–like form, such that the total low-temperature binding energy can be written as

$$U=\sum_{i,j}\varepsilon_i\{[\sigma_i/R_{ij}(\xi_k)]^{m_i}-[\sigma_i/R_{ij}(\xi_k)]^{n_i}\}\ , \qquad (1)$$

where i refers to the atom pair type (*AB*, *BA*, *AA*, or *BB*). R_{ij} is the interatomic distance of the jth member of the ith pair type and is a function of the structural parameters ξ_k. Whereas the cubic CsCl-type structure has only one ξ_k (its lattice parameter a), the orthorhombic Fe*B*—type has seven ξ_k's (three lattice parameters a,b,c plus four internal parameters x_A,z_A,x_B,z_B). Hence, if we minimize U for the latter structure with respect to each ξ_k, we obtain seven secular equations of the form,

$$F_k=\sum_{i,j}\varepsilon_i\frac{\partial R_{ij}}{\partial\xi_k}R_{ij}^{-1}[m_i(\sigma_i/R_{ij})^{m_i}-n_i(\sigma_i/R_{ij})^{n_i}]=0\ . \qquad (2)$$

For $PrAg_{0.5}Cu_{0.5}$, each R_{ij} (and $\partial R_{ij}/\partial\xi_k$) is known numerically from its dependence on the experimentally determined ξ_k's, as shown in Appendix A. Hence, with assumed values for the exponents m_i and n_i, the seven equations (2) can be solved simultaneously for the ε_i's and σ_i's; in fact, for convenient normalization we set ε_{AB} equal to unity, leaving only five variables $(\varepsilon_{AA},\varepsilon_{BB},\sigma_{AB},\sigma_{AA},\sigma_{BB})$ to be evaluated.

The problem was given to the IBM 3801K computer at the University of Illinois at Chicago via a nonlinear least-squares-fitting program, whereby solutions for the five variables were sought, for which $\sum_k F_k^2$ is minimized, the F_k in Eq. (2) being treated as a residual quantity. A serious difficulty was encountered almost immediately, regardless of the values assumed for m_i and n_i (generally near 12 and 6, respectively). Due to their pronounced nonlinearity, the secular equations produce many local binding-energy minima in the five-dimensional solution space, and the computer program is unable to discriminate among them very effectively. However, independent of the local solution being converged upon, the value obtained for ε_{BB} was consistently about 2 orders of magnitude smaller than those for ε_{AB} or ε_{AA}. The unavoidable conclusion is that the Ag(Cu)—Ag(Cu) interactions are relatively very weak—which is reflected in the widely dispersed changes in the Ag(Cu)—Ag(Cu) separation distances that accompany the cubic-to-orthorhombic transition (Fig. 2). Interestingly, this conclusion is similar to that recently drawn[14] for Li-Li interactions in LiAl, where monovalent Li and trivalent Al may be quite analogous to Ag (Cu) and Pr in $PrAg_{0.5}Cu_{0.5}$.

Thus, we were able to set $\varepsilon_{BB}=0$, thereby also removing σ_{BB} (as well as m_{BB} and n_{BB}) from the secular equations, which reduces the number of solution variables to three $(\varepsilon_{AA},\sigma_{AB},\sigma_{AA})$. This reduction resulted in a much improved computer capability for the job at hand, and we proceeded to obtain solutions corresponding to various assumed values for the m_i's and n_i's. Since the solutions

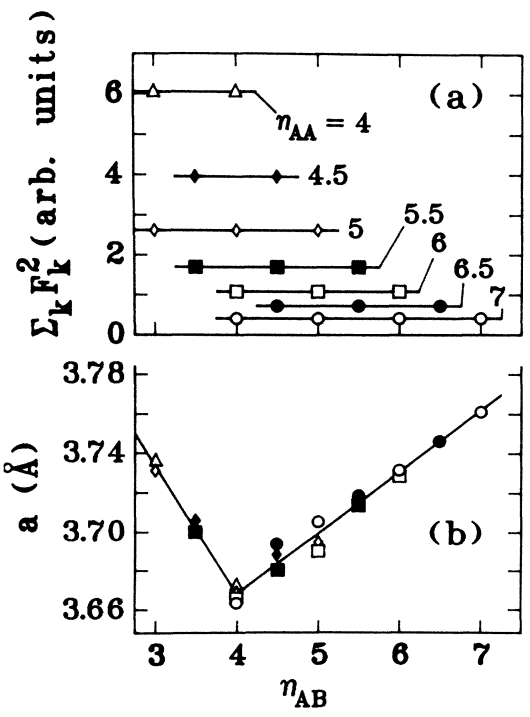

FIG. 3. Results from binding-potential calculations for (a) the residual-squared sum in arbitrary units and (b) the cubic lattice parameter in Å, as functions of n_{AB} for different n_{AA}.

were seen to be fairly insensitive to m_i values near 12, we set $m_{AB}=m_{AA}=12$ (the standard Lennard-Jones value) and focused on the effects of different values for n_{AB} and n_{AA}. In Fig. 3(a), we show $\sum_k F_k^2$ for the calculated solutions as a function of n_{AB} for various values of n_{AA}. Clearly, $\sum_k F_k^2$ is almost independent of n_{AB} but decreases rapidly with increasing n_{AA}. We then invoked another criterion, which is especially relevant to this study—namely, the lattice-parameter (a) values for the cubic phase of $PrAg_{0.5}Cu_{0.5}$ deduced by minimizing (with respect to a) the binding energy expressed in Eq. (1), in which the assumed values for n_{AB} and n_{AA} and the corresponding values for the solution variables have been inserted. The values for a for various n_{AB} and n_{AA} are shown in Fig. 3(b), where it is seen that a goes through the same minimum at the same value of n_{AB} for any value of n_{AA}. Since the minimum value of a happens to agree very closely with the experimental value of 3.66 Å, the position of the minimum is taken to give $n_{AB}=4$. We then set $n_{AA}=6$ (the other standard Lennard-Jones value), for which Fig. 3(a) shows a reasonably low $\sum_k F_k^2$. We are thus ignoring the continued decrease of $\sum_k F_k^2$ at higher n_{AA}, which is caused in part by the fact that the binding energy (U) itself decreases in magnitude as n_{AA} is allowed to approach $m_{AA}(=12)$.

With the solution variables calculated for these exponent values, the expression we obtained for the total binding energy per formula unit of $PrAg_{0.5}Cu_{0.5}$ as a summation over the A-B and A-A interatomic distances (where A=Pr, B=Ag or Cu) may be written as

$$U=2\sum_{R_{AB}} U_{AB}(R_{AB})+\sum_{R_{AA}} U_{AA}(R_{AA}) , \tag{3}$$

where

$$U_{AB}(R_{AB})=\varepsilon_{AB}[(\sigma_{AB}/R_{AB})^{12}-(\sigma_{AB}/R_{AB})^{4}]$$

and

$$U_{AA}(R_{AA})=\varepsilon_{AA}[(\sigma_{AA}/R_{AA})^{12}-(\sigma_{AA}/R_{AA})^{6}] ,$$

in which $\varepsilon_{AB}=1$ (as normalized), $\sigma_{AB}=2.716$ Å, $\varepsilon_{AA}=0.55$, and $\sigma_{AA}=3.485$ Å. In Fig. 4, $U_{AB}(R_{AB})$ and $U_{AA}(R_{AA})$ are displayed graphically to scale. Since these potentials were essentially derived from the atomic positions in the orthorhombic FeB-type structure, it is not surprising that their minima at 3.116 and 3.912 Å occur, respectively, very near the short-range A-B and A-A interatomic spacings in this structure (see Fig. 2). That the minimum of U_{AB} is deeper than that of U_{AA} is consistent with the simple fact that the compound is chemically ordered.

In Fig. 4, the solid circles on the solid curves are located at the interatomic distances for the first, second, and third nearest neighbors in the cubic CsCl-type structure of $PrAg_{0.5}Cu_{0.5}$. These distances are for the experimental lattice-parameter value of 3.66 Å which, as described above, is also the value of a that minimizes U in Eq. (3) when applied to the cubic structure. For this structure Eq. (3) gives a binding energy (U) that is slightly ($\frac{1}{2}$%) lower than that for the orthorhombic structure, consistent with the transformation evidence that the two structural

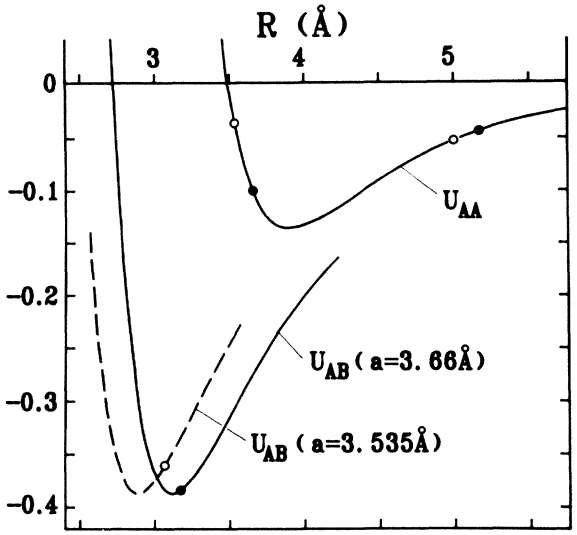

FIG. 4. Calculated curves for A-B [Pr—Ag(Cu)] and A-A (Pr-Pr) pair-binding potentials (in arbitrary units) versus interatomic distance (in Å) for $PrAg_{1-x}Cu_x$. Circled points indicate atomic positions in the CsCl-type structure for two different lattice parameters—for which U_{AB} is different but U_{AA} is the same, as shown.

phases of this compound have about the same relative stability. Note that for the first- and second-nearest-neighbor distances in the cubic structure, the points in Fig. 4 are, respectively, to the right of the $U_{AB}(R_{AB})$ minimum and to the left of the $U_{AA}(R_{AA})$ minimum. Thus, regarding these strong pair interactions, the Pr—Ag(Cu) bonds are stretched and the Pr—Pr bonds are compressed, relative to their preferred binding distances. This conflict of interest, to which the material accommodates as best it can within the cubic structure, constitutes a "structural frustration"—analogous to the spin-orientational frustration in magnetic systems such as spin glasses.

Although $PrAg_{1-x}Cu_x$ of $x>0.5$ is orthorhombic FeB-type,[12] it is pertinent to consider the consequences of artificially retaining the Cu-rich compounds in the cubic CsCl-type structure. Since the $PrAg_{1-x}Cu_x$ compounds of different x are isoelectronic, an increase of x may be regarded primarily in terms of the reduction in the cubic lattice parameter that results from the continued replacement of Ag atoms by smaller Cu atoms. Hence, it is reasonable to assume that as x increases the binding energy continues to be expressed by Eq. (3) with the same constants except for lowered values of σ_{AB}. Considering specifically the reduced lattice parameter, $a=3.535$ Å (a critical value for the phonon properties, as described later), we find that for U to be minimized at this value of a, the value of σ_{AB} must be lowered to 2.517 Å. As shown in Fig. 4, this change produces a scaled shift of the $U_{AB}(R_{AB})$ curve to lower values of R_{AB}, while the $U_{AA}(R_{AA})$ curve remains fixed. The interatomic spacings in this reduced cubic cell are represented by open circles, and it is clear from the slopes of the curves at these (and the solid circles) points that the tensile and compressive

forces on the A-B first nearest neighbors and the A-A second nearest neighbors, respectively, have both grown significantly in magnitude. Thus, the structural frustration has increased and, as we will show, this has important consequences for the phonon spectrum.

III. PHONON DISPERSIONS

With Eq. (3) for the total binding energy of $PrAg_{0.5}Cu_{0.5}$ applied to the cubic CsCl-type structure, we proceeded to determine the spatial derivatives of U_{AB} and U_{AA} that form the various force constants in the dynamical matrix of this structure. For consistency, we again restricted our analysis to interactions of atom pairs out to (and including) third nearest neighbors. Since the primitive unit cell of this structure contains two atoms, A (=Pr) and B (=Ag or Cu), both of which are at centers of inversion symmetry, the dynamical matrix ($\underline{D}$) is 6×6 and is real and symmetric. Moreover, $\underline{D}$ is composed of four 3×3 submatrices representing the A-B, A-A, and B-B pair interactions separately, i.e.,

$$\underline{D}=\begin{bmatrix}\underline{D}_{AA} & \underline{D}_{AB}\\ \underline{D}_{BA} & \underline{D}_{BB}\end{bmatrix}, \tag{4}$$

where $\underline{D}_{BA}=\underline{D}_{AB}$ and where, from our finding that the B-B interactions in $PrAg_{0.5}Cu_{0.5}$ are negligibly weak, $\underline{D}_{BB}$ is zero except for self-energy terms. The construction of the $\underline{D}_{AB}$ and $\underline{D}_{AA}$ submatrices from the force constants and the eigenvalue solutions of the $\underline{D}$ matrix for the phonon normal-mode frequencies corresponding to the principal crystallographic directions of propagation are described in Appendix B.

From the normal-mode solutions given analytically in Appendix B and using the expressions for U_{AB} and U_{AA} in Eq. (3) with the numerical coefficients pertinent to $PrAg_{0.5}Cu_{0.5}$, we computed the phonon dispersion for each of the three cubic propagation directions, $\langle 00\zeta\rangle$, $\langle\zeta\zeta 0\rangle$, and $\langle\zeta\zeta\zeta\rangle$. Our results for the various phonon branches are displayed (in arbitrary frequency units) in Fig. 5. Broadly, they resemble the phonon dispersion curves previously deduced from inelastic neutron scattering data on the CsCl-structured compounds: LaAg,[2] YZn,[15] CuZn (β-brass),[16] and CsBr,[17] but there are interesting differences. Of the various degeneracies exhibited by our calculated dispersion curves at special points [Γ (000), X ($00\frac{1}{2}$), M ($\frac{1}{2}\frac{1}{2}0$), R ($\frac{1}{2}\frac{1}{2}\frac{1}{2}$)], all but one are required by symmetry. The exception is the accidental degeneracy of the LA and TO (00ζ) branches at X, at which point an accidental degeneracy was also observed in YZn and CuZn but between the TA and TO branches. For all these other compounds, the LA branch at X was seen to lie closely above or below the TO branch, indicating that the degeneracy we find is quite coincidental.

Pertinent to the lattice instability of $PrAg_{0.5}Cu_{0.5}$ is the fact that the calculated TA(00ζ) and $TA_1(\zeta\zeta 0)$ branches in Fig. 5 lie relatively low in frequency. This suggests that the elastic constant C_{44}, which is proportional to the initial slopes squared of both these branches, may be anomalously small. Moreover, in approaching the M point, the $TA_1(\zeta\zeta 0)$ branch goes through a shallow maximum, whereas the $TA_2(\zeta\zeta 0)$ branch continues to rise monotonically before leveling out. This contrasting behavior is interesting in view of recent observations. As discussed earlier, the cubic-to-orthorhombic transition in $PrAg_{0.5}Cu_{0.5}$ involves internal atomic displacements that suggest that the cubic-phase instability corresponds to a softening of zone-boundary phonons, which in the case of ($\frac{1}{2}\frac{1}{2}0$) are those of the TA_1 mode, as seen in Fig. 1. However, it is the TA_2 mode that softens at the M point in LaAg, especially when the Ag is partially replaced by In,[2] and this mode was also seen to soften near the Γ point in PrAg.[4]

Hence, we were motivated to learn how the TA_1 and TA_2 ($\zeta\zeta 0$) phonon modes change in $PrAg_{1-x}Cu_x$ as x is raised above 0.5 while retaining artificially the cubic structure—which is analogous to the strategy adopted for the binding potentials. Specifically, for the extreme case of $x=1$ (i.e., PrCu), we considered several possible values for the cubic lattice parameter (a), starting with and rang-

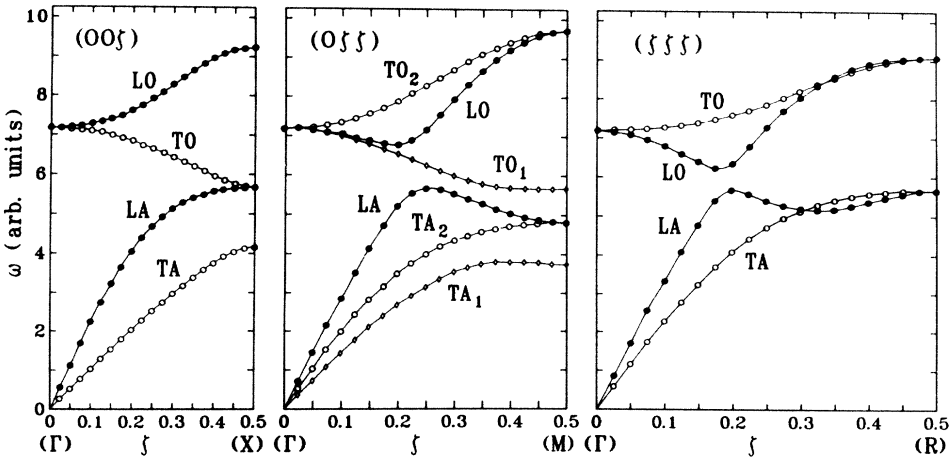

FIG. 5. Calculated phonon dispersion curves for cubic $PrAg_{0.5}Cu_{0.5}$ ($a=3.66$ Å) for propagation wave vectors (00ζ), ($\zeta\zeta 0$), and ($\zeta\zeta\zeta$), with frequency in arbitrary units. Acoustical (A) and optical (O) branches for longitudinal (L) and transverse (T) polarizations are so labeled.

TABLE I. Calculated elastic constants (in arbitrary units) for cubic $PrAg_{1-x}Cu_x$ of different x. The lattice parameters (a) and the corresponding binding-potential constants (σ_{AB}) used in the calculations are listed in angstroms.

x	a	σ_{AB}	C_{44}	C'	C_{12}	C_{11}
0	3.74	2.805	1.957	2.263	1.937	6.462
0.5	3.66	2.716	1.648	3.281	1.639	8.202
1	3.58	2.603	1.078	4.733	1.092	10.558
1	3.54	2.528	0.6365	5.686	0.6741	12.047
1	3.535	2.517	0.5713	5.818	0.6131	12.250

ing down from 3.58 Å, as derived from linear extrapolation of the experimental values of 3.74 and 3.66 Å for $x=0$ and 0.5, respectively. For each value of a, static equilibrium of the cubic phase was achieved by minimizing the total binding energy in Eq. (3) with respect to σ_{AB}, all other parameters being held fixed at their values for $x=0.5$. The σ_{AB} values found for the different a's are listed in Table I. In each case, with the binding potentials so determined, we went on as before to calculate the phonon dispersion curves from the expressions in Appendix B.

Our results for the TA_1 and TA_2 ($\zeta\zeta 0$) branches, which are of particular interest and also reveal the most significant changes, are displayed in Fig. 6, labeled by the alternative values of a for $x=1$. Also shown are the corresponding phonon branches calculated for $a=3.66$ Å ($x=0.5$) and $a=3.74$ Å ($x=0$), whose σ_{AB} values are included in Table I. It is immediately obvious from this figure that as a decreases the maximum in the TA_1 branch (originally noted in Fig. 5 as a subtle feature for $a=3.66$ Å) becomes increasingly conspicuous as the branch rapidly softens at the M point, the softening going essentially all the way to completion for $a=3.535$ Å. In fact, the entire TA_1 branch is descending, so that the elastic constant C_{44}, which equals the initial slope squared (times the density ρ), is rapidly diminishing. Contrastingly, the TA_2 branch rises with decreasing a, though some softening is starting to occur near the M point as a approaches 3.535 Å. In this case, the initial slope squared (times ρ) gives $\frac{1}{2}(C_{11}-C_{12})$ or C', whose values increase monotonically with decreasing a.

Our numerical results for C_{44} and C' are listed in Table I; also listed (in the same arbitrary units) are the C_{11} values deduced from the initial slopes of the calculated LA(00ζ) branches and the C_{12} values obtained by combining C_{11} and C'. The contrasting variations of C_{44} and C' with a are clearly evident, as is an unexpectedly close correspondence between the values of C_{44} and C_{12}. That the Cauchy relation ($C_{44}=C_{12}$) is nearly obeyed can be traced to the fact that the off-diagonal elements of the $\underline{D}_{AB}$ and $\underline{D}_{AA}$ submatrices in Appendix B are relatively weak, which implies that the interatomic forces are nearly centrosymmetric. Interestingly, the experimental values for C_{44} and C_{12} are quite close in both YZn (Ref. 15) and CuZn (Ref. 16). However, in LaAg,[1] CeAg,[3] and PrAg,[4] which pertain more directly to our study but which show the TA_2 (C') mode lying well below rather than above the TA_1 (C_{44}) mode, C_{12} was found to be about twice C_{44}. Since the electron density-of-states mechanism suggested for the softening of the TA_2 mode in the latter compounds is ignored in our calculations, it is not surprising that our own results for PrAg (Fig. 6 and Table I for $a=3.74$ Å) display no obvious signs of any phonon softening. It is only when the Ag in PrAg is progressively replaced isoelectronically by Cu, resulting in a reduced lattice parameter and an increased structural frustration, that we find that a softening develops in the TA_1 mode, especially at the M point.

The exact nature of the M-point phonon softening revealed by our calculations is readily established by setting $\theta_2=\pi/2$ in the dispersion relation for the $T_1(\zeta\zeta 0)$ modes given by Eq. (B18) of Appendix B. The roots of this quadratic equation in ω^2 become simply

$$\omega_a^2=8(\alpha_1+\beta_2+2\alpha_3)/m_A,\quad \omega_0^2=8\alpha_1/m_B\ , \tag{5}$$

for the TA_1 and TO_1 modes, respectively. α_1, β_2, and α_3 are interatomic force constants which depend on the spatial derivatives of the pair-binding potentials, as specified in Appendix B. As expected for the $\frac{1}{2}\frac{1}{2}0$ zone-boundary

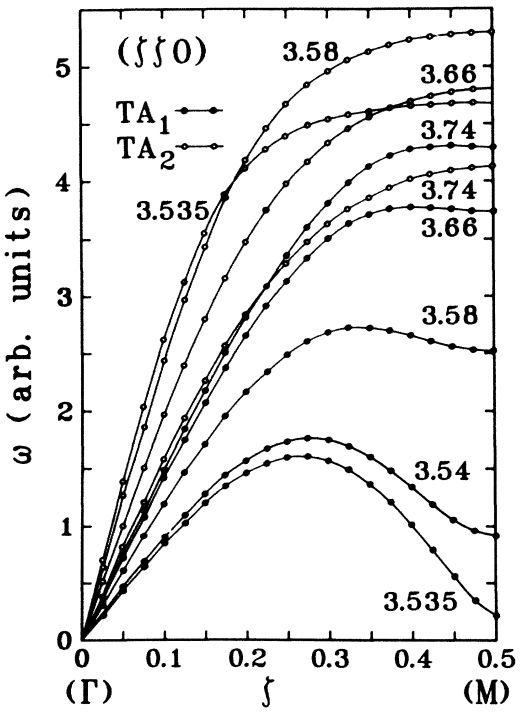

FIG. 6. Calculated phonon dispersion curves for TA_1 and TA_2 ($\zeta\zeta 0$) modes (shown by the solid and open circles, respectively) for cubic $PrAg_{1-x}Cu_x$ of different lattice parameters.

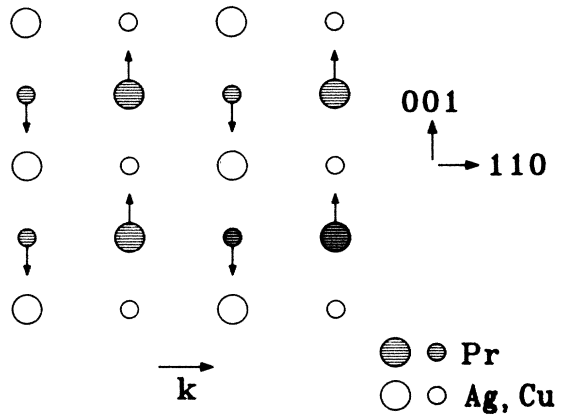

FIG. 7. Atomic vibrational pattern for TA_1 mode at the M $(\frac{1}{2}\frac{1}{2}0)$ point in cubic $PrAg_{1-x}Cu_x$. Alternating (110) planes of Pr atoms are vibrating in opposite phases along (001).

point, the masses of Pr (m_A) and Ag or Cu (m_B) appear separately in these eigenfrequency expressions, indicating that the TA_1 and TO_1 modes involve, respectively, only the motion of the heavier Pr or lighter Ag (Cu) atoms. Specifically, in the TA_1 mode which softens, the Pr atoms in alternate (110)-type planes are vibrating in opposite time phase along the ⟨001⟩ axis, while the Ag (Cu) atoms are immobile, as shown in Fig. 7. (The same situation obtains in the TO_1 mode but with the roles of the Pr and Ag (Cu) atoms interchanged). Comparing Fig. 7 with the same projection of the CsCl-type structure in Fig. 1, we see that the internal static distortions of $\frac{1}{2}\frac{1}{2}0$ symmetry that take the latter into the FeB-type structure have precisely the same pattern as the dynamic distortions of the TA_1 (or TO_1) mode at the M point. Thus, the dynamic instability of cubic $PrAg_{1-x}Cu_x$ clearly expresses itself as a precursor of the cubic-to-orthorhombic transformation that occurs at sufficiently large x. Furthermore, our finding that the TA_1 mode would soften completely (Fig. 6) if this transformation did not already occur can be easily understood from a quantitative consideration of Eq. (5). Our calculations show that as the cubic lattice parameter a approaches 3.535 Å the force constant β_2 becomes strongly negative and ultimately drives ω_a to zero. Since β_2 is proportional to $\partial U_{AA}/\partial R$ at the Pr-Pr second-neighbor separation distance (R_2), it follows from the binding-potential picture in Fig. 4 that the softening of the TA_1 mode is directly related to the increase in the negative slope of U_{AA} at R_2 which manifests the growing structural frustration in $PrAg_{1-x}Cu_x$ with increasing x.

IV. CONCLUDING REMARKS

Although our phonon-dispersion calculations are based on simple Lennard-Jones–like binding potentials, they succeed in establishing the probable nature of the lattice instability in cubic $PrAg_{1-x}Cu_x$. That our results are insensitive to all but a few essential details of the calculations is borne out by the fact that when we ignore the interactions between third nearest neighbors (as well as those previously neglected between more distant atoms) we find no significant change in the phonon spectrum. In particular, the softening of the TA_1 mode at the M point is seen to express itself almost the same as before. And the reason for this is that the first- and second-nearest-neighbor interactions are sufficient to produce the structural frustration which underlies the phonon softening.

Regarding any direct experimental verification of our calculated results, the only attempt to date has been through some ultrasonic measurements on polycrystalline samples of PrAg and $PrAg_{0.6}Cu_{0.4}$.[18] The sound velocity for transverse polarization relative to that for longitudinal polarization was found to be considerably smaller in the latter compound, which is consistent with a weakening of the elastic constant C_{44} pertinent to the TA_1 mode with increasing Cu concentration. However, these results are fairly sensitive to any preferential orientation of the crystallites in the samples, and the measurements should be repeated with single crystals. Indeed, if and when $PrAg_{1-x}Cu_x$ crystals of sufficient size become available, a more definitive test of our calculated phonon spectra would be via inelastic neutron scattering experiments. Meanwhile, our calculated results stand as a self-consistent description of the lattice instability in cubic $PrAg_{1-x}Cu_x$, which was originally suggested by the anomalously strong antiferroquadrupolar interactions in this pseudobinary system.

ACKNOWLEDGMENTS

We are very grateful to Professor J. W. Garland for many helpful discussions of various theoretical aspects of this problem. The work at the University of Illinois at Chicago was supported by the National Science Foundation under Grant No. DMR-84-06898 and at the Argonne National Laboratory by the U.S. Department of Energy, BES—Materials Sciences, under Contract No. W-31-109-Eng-38.

APPENDIX A

In the following listing for $PrAg_{0.5}Cu_{0.5}$, the Pr sites are identified as A,B,C,D and the Ag and Cu sites as a,b,c,d, in accordance with the labeling in Fig. 1. The atomic neighbors in the orthorhombic phase are listed by the number at each site, with reference to the corresponding atomic shell in the cubic phase. Their positions are specified as $(x/a,y/b,z/c)$ in terms of the internal parameters, x_A,z_A,x_B,z_B, relative to the central Pr or Ag (Cu) atom at (0,0,0), and are followed by their distances (in Å) from the central atom.

For Pr at central site A:

Cubic phase, 8 Ag or Cu atoms at $3^{1/2}a/2=3.17$ Å	
a (2) $(x_A+x_B-\frac{1}{2},\frac{1}{2},z_A-z_B+\frac{1}{2})$	3.17
b (2) $(x_A+x_B,\frac{1}{2},z_A+z_B-1)$	3.11
c (1) $(x_A-x_B-\frac{1}{2},0,z_A+z_B-\frac{1}{2})$	3.06
c (1) $(x_A-x_B-\frac{1}{2},0,z_A+z_B-\frac{3}{2})$	4.92
d (1) $(x_A-x_B,0,z_A-z_B+1)$	3.05
d (1) $(x_A-x_B,0,z_A-z_B)$	3.10

Cubic phase, 6 Pr atoms at $a=3.66$ Å

B (1)	$(\frac{1}{2},0,2z_A-\frac{1}{2})$	3.90
B (1)	$(-\frac{1}{2},0,2z_A-\frac{1}{2})$	3.90
D (2)	$(2x_A-\frac{1}{2},-\frac{1}{2},\frac{1}{2})$	3.87
D (2)	$(2x_A-\frac{1}{2},-\frac{1}{2},-\frac{1}{2})$	3.87

Cubic phase, 12 Pr atoms at $2^{1/2}a=5.18$ Å

A (2)	(0,0,1)	5.77
B (2)	(0,1,0)	4.73
C (2)	$(2x_A,-\frac{1}{2},2z_A)$	3.87
C (2)	$(2x_A,-\frac{1}{2},2z_A-1)$	5.49
C (2)	$(2x_A-1,-\frac{1}{2},2z_A)$	5.50
C (2)	$(2x_A-1,-\frac{1}{2},2z_A-1)$	6.74

For Ag or Cu at central site a,
Cubic phase, 8 Pr atoms at $3^{1/2}a/2=3.17$ Å

A (2)	$(-x_A-x_B+\frac{1}{2},\frac{1}{2},-z_A+z_B-\frac{1}{2})$	3.17
B (2)	$(-x_A-x_B,\frac{1}{2},z_A+z_B-1)$	3.11
C (1)	$(x_A-x_B-\frac{1}{2},0,z_A+z_B-\frac{1}{2})$	3.06
C (1)	$(x_A-x_B-\frac{1}{2},0,z_A+z_B-\frac{3}{2})$	4.92
D (1)	$(x_A-x_B,0,-z_A+z_B-1)$	3.05
D (1)	$(x_A-x_B,0,-z_A+z_B)$	3.10

Cubic phase, 6 Ag or Cu atoms at $a=3.66$ Å

b (1)	$(\frac{1}{2},0,2z_B-\frac{3}{2})$	3.88
b (1)	$(-\frac{1}{2},0,2z_B-\frac{3}{2})$	3.88
d (2)	$(-2x_B,\frac{1}{2},2z_B-1)$	2.91
d (2)	$(-2x_B,\frac{1}{2},2z_B-2)$	4.80

Cubic phase, 12 Ag or Cu atoms at $2^{1/2}a=5.18$ Å

a (2)	(0,0,1)	5.77
b (2)	(0,1,0)	4.73
d (2)	$(-2x_B+\frac{1}{2},\frac{1}{2},\frac{1}{2})$	4.90
d (2)	$(-2x_B+\frac{1}{2},\frac{1}{2},-\frac{1}{2})$	4.90
d (2)	$(-2x_B-\frac{1}{2},\frac{1}{2},\frac{1}{2})$	5.59
d (2)	$(-2x_B-\frac{1}{2},\frac{1}{2},-\frac{1}{2})$	5.59

In the above, for the orthorhombic phase, we have the following: $a=7.34$ Å, $b=4.73$ Å, $c=5.77$ Å; $x_A=0.179$, $z_A=0.136$, $x_B=0.034$, $z_B=0.641$.

APPENDIX B

1. Dynamical matrix

The submatrices, $\underline{D}_{AB}$, $\underline{D}_{AA}$, and $\underline{D}_{BB}$, that form the dynamical matrix of the cubic CsCl-type structure as shown in Eq. (4), were constructed following standard procedures.[19,20] Consistent with our binding-potential analysis, consideration of the atomic pair interactions was restricted to first, second, and third nearest neighbors, whose positions are specified by

$$\mathbf{R}_1,\ \mathbf{R}_2,\ \text{or}\ \mathbf{R}_3=\pm a(n_x,n_y,n_z)\ , \tag{B1}$$

where a is the cubic lattice parameter and n_x,n_y,n_z are reduced Cartesian coordinates. The corresponding Fourier transforms all contain the trigonometric function,

$$\xi(n_x,n_y,n_z)=2\cos[a(n_xk_x+n_yk_y+n_zk_z)]\ , \tag{B2}$$

where k_x,k_y,k_z are wave-vector components.

Starting with the construction of $\underline{D}_{AB}$, we need only consider the first nearest neighbors, for which $R_1=3^{1/2}a/2$ and

$$(n_x,n_y,n_z)_1=(\tfrac{1}{2},\tfrac{1}{2},\tfrac{1}{2}),\ (\tfrac{1}{2},\tfrac{1}{2},\tfrac{\bar{1}}{2})\ ,\quad (\tfrac{1}{2},\tfrac{\bar{1}}{2},\tfrac{1}{2}),\ (\tfrac{\bar{1}}{2},\tfrac{1}{2},\tfrac{1}{2})\ . \tag{B3}$$

The 3×3 matrix coefficients of the Fourier transforms, $\underline{G}(n_x,n_y,n_z)_1$, are real and symmetric, and their elements are

$$\begin{aligned} G_{11}&=G_{22}=G_{33}=\alpha_1\ ,\\ G_{12}&=G_{21}=4n_xn_y\beta_1\ ,\\ G_{23}&=G_{32}=4n_yn_z\beta_1\ ,\\ G_{13}&=G_{31}=4n_zn_x\beta_1\ , \end{aligned} \tag{B4}$$

in which the force constants, α_1 and β_1, depend on the spatial derivatives of the pair potential U_{AB} at R_1 as follows:

$$\begin{aligned} \alpha_1&=\tfrac{1}{3}(U''_{AB}+2U'_{AB}/R)_{R_1}\ ,\\ \beta_1&=\tfrac{1}{3}(U''_{AB}-U'_{AB}/R)_{R_1}\ , \end{aligned} \tag{B5}$$

where $U''=d^2U/dR^2$ and $U'=dU/dR$. Then, by a summation over the $(n_x,n_y,n_z)_1$ values in (B3), we obtain

$$\underline{D}_{AB}=(m_Am_B)^{-1/2}\sum\underline{G}(n_x,n_y,n_z)_1\xi(n_x,n_y,n_z)_1\ , \tag{B6}$$

where m_A and m_B are the atomic masses.

Similar steps are taken in constructing $\underline{D}_{AA}$ but with respect to second- and third-nearest-neighbor A-A pairs. For the second neighbors, $R_2=a$ and

$$(n_x,n_y,n_x)_2=(1,0,0),\ (0,1,0),\ (0,0,1)\ . \tag{B7}$$

The Fourier-transform matrices, $\underline{J}(n_x,n_y,n_z)_2$, are diagonal, their elements being

$$\begin{aligned} J_{11}&=n_x\alpha_2+(n_y+n_z)\beta_2\ ,\\ J_{22}&=n_y\alpha_2+(n_z+n_x)\beta_2\ ,\\ J_{33}&=n_z\alpha_2+(n_x+n_y)\beta_2\ , \end{aligned} \tag{B8}$$

in which the force constants depend on the derivatives of the potential U_{AA} at R_2 as follows:

$$\alpha_2=(U''_{AA})_{R_2},\ \beta_2=(U'_{AA}/R)_{R_2}\ . \tag{B9}$$

For the third neighbors, $R_3=2^{1/2}a$ and

$$(n_x,n_y,n_z)_3=(1,1,0),\ (1,0,1),\ (0,1,1)\ ,\quad (1,\bar{1},0),\ (\bar{1},0,1),\ (0,1,\bar{1})\ . \tag{B10}$$

The Fourier-transform matrices, $\underline{K}(n_x,n_y,n_z)_3$, are real and symmetric, and their elements are

$$
\begin{aligned}
K_{11} &= n_x^2(\alpha_3-\beta_3)+\beta_3 , \\
K_{22} &= n_y^2(\alpha_3-\beta_3)+\beta_3 , \\
K_{33} &= n_z^2(\alpha_3-\beta_3)+\beta_3 , \\
K_{12} &= K_{21} = n_x n_y(\alpha_3-\beta_3) , \\
K_{23} &= K_{32} = n_y n_z(\alpha_3-\beta_3) , \\
K_{13} &= K_{31} = n_z n_x(\alpha_3-\beta_3) ,
\end{aligned}
\tag{B11}
$$

in which the force constants depend on the derivatives of U_{AA} at R_3 as follows:

$$
\alpha_3 = \tfrac{1}{2}(U''_{AA}+U'_{AA}/R)_{R_3}, \quad \beta_3 = (U'_{AA}/R)_{R_3} . \tag{B12}
$$

Then, by the following summations over the $(n_x,n_y,n_z)_2$ values in (B7) and the $(n_x,n_y,n_z)_3$ values in (B10) plus a self-energy term involving α_1 in (B5), we obtain

$$
\underline{D}_{AA} = m_A^{-1}\left[\sum \underline{J}(n_x,n_y,n_z)_2 \xi(n_x,n_y,n_z)_2 + \sum \underline{K}(n_x,n_y,n_z)_3 \xi(n_x,n_y,n_z)_3 + 8\alpha_1 \underline{1}\right] , \tag{B13}
$$

where $\underline{1}$ is the 3×3 identity matrix.

In principle, for the CsCl-type structure, $\underline{D}_{BB}$ is completely analogous to $\underline{D}_{AA}$. However, since the potential U_{BB} is negligibly small in the present case of interest, $\underline{D}_{BB}$ reduces down to the self-energy term, i.e.,

$$
\underline{D}_{BB} = m_B^{-1}(8\alpha_1 \underline{1}) . \tag{B14}
$$

2. Phonon dispersion

From the dynamical matrix $\underline{D}$ composed of $\underline{D}_{AB}$, $\underline{D}_{AA}$, and $\underline{D}_{BB}$ as indicated in Eq. (4), eigensolutions were obtained for the phonon dispersions in the principal cubic directions of propagation. The dispersion relations are all quadratic in ω^2, the roots corresponding to the acoustical and optical branches. In terms of the various force constants and the atomic masses, we define

$$
\begin{aligned}
a_1 &= 8m_A^{-1}\alpha_1, \quad a_2 = 8m_B^{-1}\alpha_1 , \\
b_1 &= 4m_A^{-1}(\alpha_2+4\alpha_3) , \\
b_2 &= 4m_A^{-1}(\beta_2+2\alpha_3+2\beta_3) , \\
b_3 &= 4m_A^{-1}(\alpha_2+\beta_2+2\alpha_3+2\beta_3) , \\
b_4 &= 8m_A^{-1}(\beta_2+2\alpha_3) , \\
b_5 &= 4m_A^{-1}(\alpha_2+2\beta_2) , \\
c_1 &= 4m_A^{-1}\alpha_3, \quad c_2 = 4m_A^{-1}\beta_3 , \\
d_1 &= 8(m_A m_B)^{-1/2}\alpha_1, \quad d_2 = 8(m_A m_B)^{-1/2}\beta_1 .
\end{aligned}
$$

With these as coefficients, the phonon dispersion relations for the longitudinal (L) and transverse (T) branches are as follows.

For L (00ζ),

$$
\omega^4-(a_1+a_2+b_1\sin^2\theta_1)\omega^2+a_2(a_1+b_1)\sin^2\theta_1=0 . \tag{B15}
$$

For T(00ζ),

$$
\omega^4-(a_1+a_2+b_2\sin^2\theta_1)\omega^2+a_2(a_1+b_2)\sin^2\theta_1=0 , \tag{B16}
$$

where $\theta_1=\pi\zeta=\frac{1}{2}ak$.

For L($\zeta\zeta$0),

$$
\omega^4-[a_1+b_3\sin^2\theta_2+(2c_1-c_2)\sin^2(2\theta_2)](\omega^2-a_2) - a_2\omega^2-(d_1\cos^2\theta_2-d_2\sin^2\theta_2)^2=0 . \tag{B17}
$$

For T$_1$($\zeta\zeta$0),

$$
\omega^4-[a_1+b_4\sin^2\theta_2+c_2\sin^2(2\theta_2)](\omega^2-a_2) - a_2\omega^2-(d_1\cos^2\theta_2)^2=0 . \tag{B18}
$$

For T$_2$($\zeta\zeta$0),

$$
\omega^4-[a_1+b_3\sin^2\theta_2+c_2\sin^2(2\theta_2)](\omega^2-a_2) - a_2\omega^2-(d_1\cos^2\theta_2+d_2\sin^2\theta_2)^2=0 , \tag{B19}
$$

where $\theta_2=\pi\zeta=\frac{1}{2}ak/2^{1/2}$.

For L($\zeta\zeta\zeta$),

$$
\omega^4-[a_1+b_5\sin^2\theta_3+(4c_1-c_2)\sin^2(2\theta_3)](\omega^2-a_2) - a_2\omega^2-(d_1\cos^2\theta_3-2d_2\sin^2\theta_3)^2\cos^2\theta_3=0 . \tag{B20}
$$

For T($\zeta\zeta\zeta$),

$$
\omega^4-[a_1+b_5\sin^2\theta_3+(c_1+2c_2)\sin^2(2\theta_3)](\omega^2-a_2) - a_2\omega^2-(d_1\cos^2\theta_3+d_2\sin^2\theta_3)^2\cos^2\theta_3=0 , \tag{B21}
$$

where $\theta_3=\pi\zeta=\frac{1}{2}ak/3^{1/2}$.

[1] W. Assmus, R. Takke, R. Sommer, and B. Lüthi, J. Phys. C **11**, L575 (1978).

[2] K. Knorr, B. Renker, W. Assmus, B. Lüthi, R. Takke, and H. J. Lauter, Z. Phys. B **39**, 151 (1980).

[3] R. Takke, N. Dolezal, W. Assmus, and B. Lüthi, J. Magn. Magn. Mater. **23**, 247 (1981).

[4] M. Giraud, P. Morin, J. Rouchy, D. Schmitt, and E. du Trémolet de Lacheisserie, J. Magn. Magn. Mater. **37**, 83 (1983).

[5] J. Maetz, M. Müllner, H. Jex, W. Assmus, and R. Takke, Z. Phys. B **37**, 39 (1980).

[6] H. Ihrig and W. Lohmann, J. Phys. F **7**, 1957 (1977).

[7] K. Yagasaki, Y. Uwatoko, Y. Kadena, H. Fujii, and T. Okamoto, J. Phys. F **15**, 651 (1985).

[8] T. O. Brun, J. S. Kouvel, and G. H. Lander, Phys. Rev. B **13**, 5007 (1976).

[9] P. Morin and D. Schmitt, Phys. Rev. B **26**, 3891 (1982).

[10] G. A. Gehring and K. A. Gehring, Rep. Prog. Phys. **38**, 1

(1975).
[11]J. A. Gotaas, J. S. Kouvel, T. O. Brun, and J. W. Cable, J. Magn. Magn. Mater. **36**, 208 (1983).
[12]J. A. Gotaas, J. S. Kouvel, and T. O. Brun, Phys. Rev. B **32**, 4519 (1985).
[13]J. W. Garland (private communication).
[14]T. O. Brun, J. E. Robinson, S. Susman, D. F. R. Mildner, R. Dejus, and K. Sköld, Solid State Ionics **9-10**, 485 (1983).
[15]T. S. Prevender, S. K. Sinha, and J. F. Smith, Phys. Rev. B **6**, 4438 (1972).
[16]G. Gilat and G. Dolling, Phys. Rev. **138**, A1053 (1965).
[17]S. Rolandson and G. Raunio, Phys. Rev. B **4**, 4617 (1971).
[18]I. Abu-Aljarayesh, D. M. Hwang, and J. S. Kouvel, Bull. Am. Phys. Soc. **29**, 321 (1984).
[19]G. L. Squires, in *Inelastic Scattering of Neutrons in Solids and Liquids* (International Atomic Energy Agency, Vienna, 1963), Vol. II, p. 71.
[20]A. A. Maradudin, in *Dynamical Properties of Solids,* edited by G. K. Horton and A. A. Maradudin (North-Holland, Amsterdam, 1974), Vol. 1.